OSCILLATORY INSTABILITIES OF THE LIQUID AND MUSHY LAYERS DURING SOLIDIFICATION OF ALLOYS UNDER ROTATIONAL CONSTRAINT

T.L. Sayre and D.N. Riahi
Departments of Theoretical and Applied Mechanics
(216 Talbot Laboratory, 104 S. Wright St.) and
Mechanical and Industrial Engineering
(138 Mechanical Eng. Bldg. 1206 W. Green St.)
University of Illinois, Urbana, IL 61801

SUMMARY

Linear flow instabilities due to oscillatory disturbances of the liquid and mushy regions during solidification of binary alloys are investigated under a rotational constraint where the rotation axis is inclined to the gravity vector. Results of stability analyses and numerical computations for a preferred centrifugal mode of general oscillatory disturbances at zero and non-zero rotation rates are determined which provide information about the preference of oscillatory flow and its role on the solidification system as modified by the rotational effects. The main results are due to a preferred oscillatory mode of convection which is more significant for non-zero rotation case and is restricted mostly to the mushy region. The preferred oscillatory mode of convection is a traveling wave in the presence of rotation, but it is a standing wave in the absence of rotation. The results for different Prandtl numbers indicate that the freckles formation tendency for metallic alloys is less than that for aqueous solutions. Freckles are imperfections that reduce the quality of the solidified materials.

1. Introduction

Recently Worster [1] investigated instabilities of the liquid and mushy regions during unidirectional solidification of alloys and in the absence of any rotational effects. He studied only the onset of non-oscillatory instabilities. He stated in his paper [1] that oscillatory instabilities are not expected to occur in his solidification system since double-diffusive systems in which the lower diffusing component is unstably stratified, such as his system, usually give way to direct modes of instability that lead to the formation of double-diffusive fingers. Accordingly, he superimposed non-oscillatory disturbances on the base flow and performed a linear stability analysis of the problem. Most of his results are for the cases of aqueous solutions whose representative Prandtl number Pr is $Pr = 10$, while the rest of his results are for the cases of metallic alloys whose appropriate Prandtl number is $Pr = 0.02$. Worster [1] discovered two modes of convection and called them appropriately the mushy layer mode and the boundary layer mode. The mushy layer mode is driven by buoyant residual fluid within the mushy layer of dendrite crystals, while the boundary layer mode is associated with a thin compositional boundary layer in the melt just above the mush-liquid interface. Depending on the parameter values, due to thermodynamic and physical properties of the alloy, either one of these modes can dominate. Worster [1] determined various results including marginal stability curves for different parameter values and found good agreement between his results of linear stability analysis for $Pr = 10$ and the experimental results of Tait and Jaupart [2] for the onset of the mushy layer mode of convection in aqueous solutions of ammonium chloride.

More recently Sayre and Riahi [3] investigated non-oscillatory instabilities of the liquid and mushy regions during solidification of binary alloys under a high gravity environment, where it was assumed that the solidification system was placed in a centrifuge basket [4] whose rotation axis was inclined with respect to the high gravity vector. The high gravity vector was also assumed to be anti-parallel to the direction of the solidification growth rate. They considered a linear stability system due to two-dimensional non-oscillatory disturbances and developed a numerical code which was used to determine the results for various flow features due to the preferred stationary instability modes of the stability system. Their results indicated two preferred distinct modes of stationary convection whose characteristics are no longer of the kind detected by Worster [1] since rotational effects altered significantly the form of these modes. They appropriately called these two modes short wavelength and long wavelength modes since they had distinct short and long wavelength characteristics which persisted even in the case of strong rotation. They found that rotational effects made both of these stationary modes more dependent on the internal structure of the mushy layer and resulted in the production of negative perturbations of the solid fraction within the mushy layer that are indicative of freckle formation tendencies, although the long wavelength mode was found to be more effective in such production processes. The spatial locations in the mushy region which tended to form freckles were found to change as the rotation rate decreased or increased. This led the authors to suggest a controlling procedure for the possible elimination of freckles, namely application of a variable rotation rate.

In the present investigation, we consider the same marginal stability problem as the one studied earlier [3], but for the oscillatory disturbances, and for the case where the solidification growth rate direction is anti-parallel to the normal gravity vector and is inclined to the rotation axis. This system turns out to be mathematically the same as the high gravity system treated before by the present authors [3], provided that the Rayleigh numbers are defined based on the acceleration due to normal gravity g and not based on the magnitude of the high gravity vector. An interesting result of the present study, in contrast to the ones due to stationary instability cases [1,3], is the persistence of a preferred oscillatory mode which is favored more by rotational constraint, by the metallic alloys and by the mushy region.

2. Formulation

We consider a thin layer of a binary alloy melt of some constant composition C_0 and temperature T_∞ which is solidified at a constant rate V_0, with the eutectic temperature T_e at the position $z = 0$ held fixed in a frame moving with the solidification speed in the vertical z-direction (anti-parallel to the gravity vector) (figure 1). The physical model is based on the assumptions of the type considered by Worster [1], and we refer the reader to this reference for details of such assumptions. We assume that the solidification system is rotating at some constant angular velocity Ω about the rotation axis which makes an angle γ with respect to the z-axis. Within the layer of melt, there is a very thin mushy layer adjacent to the solidifying surface and of thickness $h(x,y,t)$, where t is the time variable, and x and y are the horizontal variables.

Next, we consider the equations for momentum, continuity, heat and solute for both the liquid region $(z > h)$ and mushy region $(0 < z < h)$ in the moving frame $0xyz$ whose origin 0 is centered on the solid-mush interface $(z = 0)$, which is assumed to be flat [1]. The governing system of equations is non-dimensionalized using V_0, K/V_0, K/V_0^2, $\beta \Delta C \rho_0 g \mathrm{K}/V_0$, ΔC and ΔT as scales for velocity, length, time, pressure, solute and temperature, respectively. Here K is the thermal diffusivity, ρ_0 is a reference (constant) density, $\beta = \beta^* - \Im \alpha^*$, where α^* and β^* are the expansion coefficients for heat and solute respectively and $\Im$ is the slope of the liquidus curve [1], which is assumed to be constant, $\Delta C \equiv C_0 - C_e$, C_e is the eutectic concentration of the alloy, $\Delta T \equiv T_L(C_0) - T_e$, and T_L is the local liquidus temperature. Due to the variations of density with respect to solute concentration and temperature, the centrifugal acceleration terms in the momentum equations for both the liquid and mushy layers cannot be converted into passive gradient terms and become important at significant rotation rates. In this paper, we are particularly interested in the effects of these terms on the solidification system. Some recent results due to Riahi [5], based on an evolution equation for the flow of melt in a solidification system, in the absence of mushy layer, indicate that there can be unusual and unexpected effects due to the centrifugal acceleration term. Following [1,6], we treat the mushy layer as a porous medium where Darcy's law is adopted.

The non-dimensional form of the governing equations and the boundary conditions for the liquid and mushy layers are based on the Worster [1] simplifying assumptions that $\beta = \beta^*$, the temperature contribution to the buoyancy in the liquid zone is negligible and $\mathrm{K} >> D$, where D is the solute diffusivity. Full details of the governing system of equations and the boundary conditions for the case without rotational constraints are given in [1], while those with rotational constraints are given in [3]. We shall present the governing stability system briefly here and refer the reader to [1] for details on the solidification system and to [3] for the rotating extension. Also, details regarding convection in a rotating system are given in Chandra Sekhar [7]. We consider two-dimensional solutions of the governing system of equations for momentum, continuity (incompressible case), temperature and solute concentration for both the liquid and mushy layers and the associated boundary conditions in the (x, z) plane, which simplified mathematically this complicated governing system. The two-dimensional flow case will not include the Coriolis force terms, but it will include the centrifugal force terms to represent the rotational constraint applied on the system. It was found convenient to eliminate the pressure gradient terms in the momentum equations by considering the curl of these equations. Next, we seek solutions of the form

$$\begin{pmatrix}\theta\\ S\\ \underset{\sim}{u}\\ \phi\end{pmatrix}=\begin{pmatrix}\theta_0(z)\\ S_0(z)\\ 0\\ \phi_0(z)\end{pmatrix}+\begin{pmatrix}\theta_1(z)\\ S_1(z)\\ \underset{\sim 1}{u}(z)\\ \phi_1(z)\end{pmatrix}\exp[i(\omega t+\alpha x)]+\begin{pmatrix}\theta_2(x,z,t)\\ S_2(x,z,t)\\ \underset{\sim 2}{u}(x,z,t)\\ \phi_2(x,z,t)\end{pmatrix}, \tag{1}$$

where $\underset{\sim}{u}=(u,v,w)$ is the velocity vector, S is the solute concentration, θ is the temperature, ϕ is the local solid fraction of the mushy layer, i is the pure imaginary number $\left(\sqrt{-1}\right)$, ω is the frequency of the perturbation, α is the wave number of the perturbation, quantities with subscript '0' denote base flow quantities whose expressions are given in [1,3] and will not be repeated here, and perturbation quantities with subscripts '1' and '2' are small in comparison with the base flow quantities.

Next, using (1) in the governing system, multiply each equation and boundary condition by $\exp[-i(\omega t+\alpha x)]$, linearize the system with respect to the amplitude of the perturbations, and then take the average of the resulting system with respect to the x variable. We shall investigate numerically the following resulting system of equations and boundary conditions in the limit of zero value of the quantities with subscript '2'. In the liquid region $(z>h)$, the equations are

$$\begin{aligned}&\left[D_3^2+(D_3-i\omega)/\mathrm{P}_r-\alpha^2\right]\Omega_1+\alpha^2R_tS_1+i\alpha A_t\sin\gamma\\ &\qquad(z\cos\gamma D_3+\cos\gamma+i\alpha z\sin\gamma)S_1=0,\end{aligned} \tag{2}$$

$$\left(\varepsilon D_3^2+D_3-i\omega-\varepsilon\alpha^2\right)S_1=W_1D_3S_0, \tag{3}$$

$$\left(D_3^2-\alpha^2\right)W_1=\Omega_1, \tag{4}$$

$$\left(D_3^2 + D_3 - i\omega - \alpha^2\right)\theta_1 = W_1 D_3 \theta_0, \tag{5}$$

where $D_3 \equiv \dfrac{d}{dz}$, Ω_1 represents the perturbation vorticity, $\mathrm{Pr} = \mu/\mathrm{K}$ is the Prandtl number, μ is the Kinematic viscosity, $R_l = \beta^* \Delta C g \mathrm{K}^2 / \left(V_0^3 \mu\right)$ is the liquid solutal Rayleigh number, $A_l = \beta \Delta C \Omega^2 \mathrm{K}^3 / \left(V_0^4 \mu\right)$ is the liquid centrifugal parameter and $\varepsilon = D/\mathrm{K}$ is the inverse of the Lewis number. These equations are subjected to the following boundary conditions:

$$\theta_1 - S_1 = \left[W_1\right] = D_3 W_1 = D_3\left(S_1 - \theta_1\right) + (\varepsilon - 1)\eta_1 D_3 \theta_0 / \varepsilon = 0 \text{ at } z = h_0, \tag{6}$$

$$\theta_1 \to 0,\ S_1 \to 0,\ W_1 \to 0,\ D_3 W_1 \to 0 \text{ as } z \to \infty, \tag{7}$$

where h_0 is the unperturbed mush-liquid interface at the fixed (constant) z level, $\eta_1(x,t) = \left(h - h_0\right)$ exp $\left[-i(\omega t + \alpha x)\right]$ and the square brackets denote the jump in the enclosed quantity across the interface. In the mushy region $(0 < z < h)$, the equations are

$$\left\{D_3^2 + \left[1 + S_t\left(C_r - \theta_i\right)/\left(C_r - \theta_0\right)^2\right]\left(D_3 - i\omega\right) + 2S_t\left(C_r - \theta_i\right)D_3\theta_0/\left(C_r - \theta_0\right)^3 - \alpha^2\right\}$$

$$\theta_1 = S_t \xi_1 D_3 \theta_0 / \left(C_r - \theta_0\right)^2 + \left[1 + S_t/\left(C_r - \theta_0\right)\right] W_1 D_3 \theta_0, \tag{8}$$

$$\left\{D_3^2 - \left(\Pi'(\chi_0)\left(C_r - \theta_i\right)D_3\theta_0 / \left[\Pi(\chi_0)\left(C_r - \theta_0\right)^2\right]\right)D_3 - \alpha^2\right\}W_1 = \alpha^2 \Pi_0 R_m \theta_1$$

$$+ i\alpha \Pi_0 \sin\gamma A_m\left(\cos\gamma z D_3 + \cos\gamma + i\alpha \sin\gamma z\right)\theta_1, \tag{9}$$

$$\left(D_3 - i\omega\right)\xi_1 = W_1 D_3 \theta_0, \tag{10}$$

where $\theta_i = \varepsilon\theta_\infty/(\varepsilon-1)$, θ_∞ is the non-dimensional T_∞, $S_1 = \theta_1[1,3]$, $\xi_1 = \chi S_1 + \phi_1 C_r$, $\chi = 1-\phi$ is the liquid fraction, $\chi_0 = (C_r-\theta_i)/(C_r-\theta_0)$ is the unperturbed porosity, Π' denotes derivative of Π with respect to χ, Π_0 is a constant reference value for Π which will be set equal to one later in the numerical procedure, $S_t = L/(C\Delta T)$ is the Stefan number, C is the specific heat per unit volume, L is the latent heat of solidification per unit volume, $C_r = (C_s - C_0)/\Delta C$ is a concentration ratio, C_s is the composition of the solid phase forming the dendrites, Π is the permeability of the mushy layer, $R_m = \beta\Delta C g\Pi_0^*/(V_0\mu)$ is the mush solutal Rayleigh number, Π_0^* is a reference value of the permeability and $A_m = \beta\Delta C\Pi_0^* \mathrm{K}\Omega^2/(V_0^2\mu)$ is the mush centrifugal parameter. These equations are subjected to the following boundary conditions:

$$[\theta_1] = [D_3\theta_1] + S_t\eta_1 D_3\theta_0/(C_r-\theta_i) = \xi_1 - \theta_1 - \eta_1 D_3\theta_0 = 0 \ \text{ at } z = h_0, \tag{11}$$

$$R_t D_3 W_1\big|_{mush} = -R_m\Pi(1)\left[D_3\Omega_1 + (\Omega_1 + \alpha^2 W_1)/P_r\right]_{liquid} \ \text{ at } z = h_0, \tag{12}$$

$$\theta_1 = W_1 = 0 \ \text{ at } z = 0. \tag{13}$$

3. Numerical method

Due to the complexity of the system (2)-(13), we use a numerical procedure of the type developed and utilized by Worster [1] and based on the numerical code of Sayre and Riahi [3]. Here we describe the numerical approach briefly and refer the reader to [1,3] for details of the procedure. Define

$$\tau = \theta_\infty - \theta_0 \qquad\qquad (0 \le \tau \le \tau_e) \tag{14}$$

as the new independent variable, where $\tau_e \equiv 1 + \theta_\infty$, and $\tau = 0$ and τ_e correspond, respectively, to $z = \infty$ and 0. Using (14) in (2)-(13) leads to a system of ordinary differential equations for W_1, Ω_1, θ_1, S_1 and ξ_1 as functions of the independent variable τ. Following [1,3], we find

$$R_l / R_m = A_l / A_m = H, \tag{15}$$

where H is generally a large parameter [1]. The new form of the stability system has a regular singular point at $\tau = 0$ [1]. Following [1,3], we write

$$\left(\theta_1, S_1, W_1, \Omega_1\right) = \tau^m \left(\tilde{\theta}, \tilde{S}, \tilde{W}, \tilde{\Omega}\right) \qquad 0 < \tau < \tau_i, \tag{16}$$

in the liquid region, where $\tau_i \equiv \theta_\infty/(1-\varepsilon)$ corresponds to value of $z = h_0$ and m is a root of the indicial equation. We then use the numerical procedure to solve for the analytic functions $\left(\tilde{\theta}, \tilde{S}, \tilde{W}, \tilde{\Omega}\right)$. Using (16) in the governing equations in the liquid region leads to four linearly independent solutions that satisfy the boundary conditions at $\tau = 0$ corresponding values of m [1,3] designated here by $m_i (i = 1,2,3,4)$. When $m = m_i$, the corresponding values of $\left(\tilde{\theta}, \tilde{S}, \tilde{\Omega}, \tilde{W}\right)$ at $\tau = 0$ are found from (7) and the governing equations for these variables. Also, for each value of $m = m_i$, a Taylor series expansion of the governing equations for these variables about $\tau = 0$ was applied to determine the first three derivatives of these variables at $\tau = 0$. These results allowed numerical evaluation of the governing equations for $\left(\tilde{\theta}, \tilde{S}, \tilde{\Omega}, \tilde{W}\right)$ in the liquid region to be started from the asymptotic expressions for the dependent variables near $\tau = 0$. We applied an efficient fourth-order Runge-Kutta scheme for this purpose. For each value of m_i, the governing equations were integrated from $\tau = 0$ to $\tau = \tau_i$. Next, we used (6) and (11)-(12) to relate the dependent variables in the mushy layer at $\tau = \tau_i$ to the dependent variables in the liquid region. These values are used to start the numerical integration of the equations for $\left(\theta_1, \xi_1, W_1\right)$ in the mushy layer at $\tau = \tau_i$, which continues until $\tau = \tau_e$. Note that $S_1 = \theta_1$ in the mushy layer [1,3] and there is no need for separate equations for Ω_1 since Ω_1 is given in terms of W_1 and $D_3^2 W_1$ like (4). However, the resulting solution will not, in general, satisfy all the boundary conditions. The remaining boundary conditions are used to compute the following residuals r_{ij} corresponding to index m_i:

$$r_{i1} = \tau^{m_i}\left(\tilde{\theta} - \tilde{S}\right),\ r_{i2} = \tau^{m_i}\frac{d\tilde{w}}{d\tau} + m_i\tau^{m_i-1}\tilde{w} \text{ at } \tau = \tau_i. \tag{17}$$

$$r_{i3} = \theta_1,\ r_{i4} = w_1 \text{ at } \tau = \tau_e \tag{18}$$

The determinant of the matrix $\left[r_{ij}\right]$,

$$Det = Det\ \left(R_m, \alpha, \omega; \varepsilon, H, P_r, S_t, C_r, \theta_\infty, A_m, \gamma\right), \tag{19}$$

is then computed, and R_m is varied until $Det = 0$. The corresponding solutions are eigen functions of the stability system which represent the marginally stable states of the system.

4. Results

Following [1,3], we set $\gamma = 30^\circ$, $S_t = C_r = \theta_\infty = 1$ and $\Pi(\chi) \equiv 1$. The eigen value relation $Det = 0$ then provides a marginal stability curve $R_m(\alpha)$ or $R_m(\omega)$ for each choice of values of other parameters. The parameter ε is typically very small, while H is typically very large [1]. Two different values of $\mathrm{Pr} = 10$ and 0.02 will be considered which correspond to aqueous solutions and metallic alloys, respectively. The centrifugal parameter A_m will be assigned the values 0 and 0.1 which turns out to provide adequately the absence and presence of the centrifugal force effects. The values for ε and H are similar to those chosen in [1].

The results for neutral stability curves, R_m versus α, in the absence of rotation $(A_m = 0.)$ for $\mathrm{Pr} = 10$ $\left(\omega = 0, H = 10^5, \varepsilon = 0.025\right)$ and $\mathrm{Pr} = 0.02$ $\left(\omega = 1.6, H = 10^6, \varepsilon = 0.01\right)$ are shown in figure 2. The system is unstable in the region above each curve and is stable below the curve. Just as in the case treated in [1] for $\mathrm{Pr} = 10$, the marginal curve for $\mathrm{Pr} = 10$ has two minima, corresponding to two distinct modes of convection which are both non-oscillatory. However, for $\mathrm{Pr} = 0.02$, the marginal stability curve has a minimum which corresponds to an oscillatory mode of convection. This oscillatory mode is preferred over the non-oscillatory modes $(\omega = 0)$ and corresponds to $\omega = 1.6$ or $\omega = -1.6$ since the stability system was found numerically to be insensitive with respect to the sign of ω as long as rotational effects are absent $(A_m = 0)$. It is seen from figure 2 that the system for $\Pr = 0.02$ can be more unstable than the one for $\Pr = 10$ in a certain range of the wavelengths of the convection modes. More extensive computations carried out in the present study to determine R_m versus ω confirm the results stated above for the $A_m = 0$ case. The corresponding results for the non-zero rotation case $(A_m = 0.1)$ are also determined. We found that there are two preferred oscillatory modes of convection with distinct different wavelengths and periods. Comparing these results with those due to $A_m = 0$ case, we find that rotation is destabilizing since the preferred oscillatory modes for $A_m = 0.1$ correspond to smaller R_m than the ones for the $A_m = 0$ case. It is also found that R_m values for the marginal curve are no longer symmetric with respect to the $\omega = 0$ axis when rotational effects are non-zero. The plot of R_m versus ω for marginal curve given by figure 3 indicates that the preferred oscillatory mode has a small wavelength and that α increases with A_m. This latter result as well as results about marginal stability curves for fixed values of $H = 10^6$ and $\varepsilon = 0.01$ were provided by additional computations. These results indicate that the case with $\Pr = 0.02$ corresponds to smaller R_m without rotation, while the case with $\Pr = 10$ corresponds to smaller R_m with rotation.

Streamlines for the preferred convection modes corresponding to the local minima of some neutral stability curves are presented in figures 4 and 5 for $A_m = 0,\ 0.1$ and $\Pr = 0.02,\ 10$. It is seen from these figures that rotation tends to make the convection cells slightly inclined with respect to the z-axis. The preferred oscillatory modes tend to be more concentrated close to the solid-mush interface, while the preferred stationary modes tend to be more concentrated close to the liquid-mush interface. Other results, not shown in any figures, indicate that for the preferred stationary modes, fluid flows deeply in the liquid and mushy zones for the long wavelength mode, while flow is restricted to a thin region about the mush-liquid interface for the short wavelength mode. For the preferred oscillatory modes, fluid flows in both the liquid and mushy zones for the long wavelength mode, while flow is restricted to the mushy zone for the short wavelength modes.

We also determined information about the vertical velocity and horizontal velocity in both the liquid and mushy layers and for both zero and non-zero rotation cases. It is found that the magnitude of velocity in the liquid region is generally larger than the corresponding one in the mushy region for the stationary modes, while the opposite is generally true for the oscillatory modes unless the wavelength of the mode is long.

Density plots of the perturbation to the solid fraction in the mushy region for the preferred convection modes and $A_m = 0$, 0.1 and $\mathrm{Pr} = 0.02$, 10 are shown in figures 6 and 7. Dark and light regions correspond, respectively, to regions of local melting and enhanced solidification. It is seen from these figures, as well as from further computations, that the rotational constraint, low Prandtl number fluid, and short wavelength modes all lead to some decrease in the amount of negative perturbation to the solid fraction, which means less tendency for channel formation in the mushy region. The information provided by these figures for both zero and non-zero values of A_m indicate that the spatial locations in the mushy layer which tend to form chimneys, that is dark regions in the figures corresponding to negative perturbation to the solid fraction that represent local melting of the dendrites, change as the rotation rate changes.

Some of the results discussed so far for $\mathrm{Pr} = 10$ are for fixed values of either $\varepsilon = 0.025$ and $H = 10^5$ or $\varepsilon = 0.01$ and $H = 10^6$. It turns out that the relative stability of the preferred convection modes varies considerably with the values of H and ε. A particular interpretation of H is as a measure of the relative mobility of the fluid in the melt region to that in the mushy layer [1]. Thus, increasing H causes the melt region to become more unstable relative to the mushy layer. The results from the marginal stability curves for various values of H with fixed $\varepsilon = 0.025$ and $\mathrm{Pr} = 10$ were also determined and confirm such interpretation of the parameter H. For non-zero rotation, it was found that the preferred oscillatory mode remains almost unchanged for $H \geq 6.4 \times 10^4$. This range of values for H may be called the asymptotic range where the preferred convection mode is insensitive with respect to H. Hence, a rotational constraint reduces the destabilizing effect of H.

In regard to the variation of ε, it should be noted that the main effect of such variation is to change the thickness of the compositional boundary layer ahead of the mush-liquid interface relative to the depth of the mushy layer. The thickness of the compositional boundary layer decreases with decreasing ε [1]. Marginal stability curves for several values of ε with fixed $H = 10^5$ and $\Pr = 10$ and for $A_m = 0,\ 0.1$ were also determined from the present computation. It was found that the preferred convection mode becomes more stabilized as ε decreases, and this is more strongly true for the zero rotation $(A_m = 0)$ case. Also, rotation is clearly destabilizing.

5. Discussion

The results of the present investigation indicate that centrifugal force effects can significantly affect the critical conditions and the flow structure in both the liquid and mushy layers. Centrifugal force is destabilizing in the sense that the critical values of R_m for the marginal stability curves are reduced. But, the centrifugal force seems to have beneficial effects in the sense that it appears to reduce the tendency of the flow to form freckles. Our stability analysis detected an oscillatory mode of convection which is preferred for $A_m \neq 0$ and for low $\Pr$, zero-rotation $(A_m = 0)$ cases. This result is in sharp contrast to the large $\Pr$, zero-rotation $(A_m = 0)$ cases as well as to the results due to Sayre and Riahi [3] for stationary instabilities. In both of these latter cases, two preferred stationary modes of convection occurred and were called [3] short wavelength and long wavelength modes, since they had distinct short and long wavelength characteristics.

One of the present results that the oscillatory mode of convection can be preferred at $\Pr = 0.02$ even for zero-rotation cases is an unexpected result. One does not expect for oscillatory instability to take place in zero-rotation cases of double-diffusive, one-layer systems in which the slower diffusing component is unstably stratified, such as in the liquid layer or mushy layer we have here. Such system usually gives way to a direct mode instability that leads to the formation of double-diffusive fingers [1]. However, the present system is a two-layer system which is subjected to more instabilities, particularly for low Prandtl number cases, that seems to be dominated leading to the preference of the oscillatory mode of convection for metallic alloys.

In this paper, we did a lengthy and tedious search to find the preferred convection modes at mostly non-zero frequencies, ω. We had to determine R_m as function of all the other parameters including α and ω and to investigate to see which cases lead to the smallest R_m. Of course, there is an infinite number of possibilities for ω, but we stopped searching for each case, after arriving at some kind of trend where we did not expect to detect a more critical mode of instability. Hence, although we do not have any rigorous proof that there are no more critical modes of instability beyond these which we already found, we can state here that it will be unlikely to have more critical modes of instability other than those which are already presented in this paper.

An interesting result of the present rotational studies due to the centrifugal force is that the spatial locations in the mushy layer which tend to form freckles change as the rotation rate changes. This result suggests an important industrial operational procedure for the possible elimination of freckle formation: the application, a variable rotational rate constraint imposed on the solidifying system.

It is of interest to note from the stability system (2)-(13) that rotational effects disappear for $\gamma = 0$. That is, the rotational constraint is effective here only if the rotation axis is inclined to the vertical z-axis which is anti-parallel to the gravity vector. This result emphasizes the significance of the non-vertical component of the rotation axis which carries an effective component of the centrifugal force.

Finally a note regarding the type of the preferred oscillatory mode predicted in the present study: As was presented in the previous section, we found that the preferred oscillatory solution remains unchanged with respect to a change in the sign of the frequency in the absence of rotation, although it changes, generally, in the presence of rotation. This result implies that the preferred oscillatory solution is a mode of convection in the form of a standing wave in the absence of rotation, while the preferred oscillatory solution is a mode of convection in the form of a traveling wave in the presence of rotation [8].

References

[1] Worster, M.G., Instabilities of the liquid and mushy regions during solidification of alloys. *J. Fluid Mech.*, **237**, 649-669 (1992).

[2] Tait, S., Jaupart, C., Compositional convection in a reactive crystalline mush and the evolution of porosity. Submitted for publication (1993).

[3] Sayre, T.L., Riahi, D.N., Effect of rotation on flow instabilities during solidification of a binary alloy. Submitted for publication (1995). Also appeared as TAM Report No. 784, UILU-ENG-95-6006, 1-64 (1995).

[4] Arnold, W.A., Wilcox, W.R., Carlson, F., Chait, A., Regel, L.L., Transport modes during crystal growth in a centrifuge. *J. Crystal Growth*, **119**, 24-40 (1992).

[5] Riahi, D.N., Effects of Coriolis and centrifugal forces on the melt during directional solidification of a binary alloy. Material Processing in High Gravity, edited L.L. Regel and W.R. Wilcox, (Plenum Publishing Corp.) 133-137 (1994).

[6] Roberts, P.H., Loper, D.E., Towards a theory of the structure and evolution of a dendrite layer. In Setellar and Planetary Magnetism, edited A.M. Soward, (Gordon and Breach) 329-349 (1983).

[7] Chandrasekhar, S., Hydrodynamic and Hydromagnetic Stability (Oxford University Press) (1961).

[8] Riahi, D.N., Weakly nonlinear oscillatory convection in a rotating fluid. *Proc. R. Soc. Lond. A.*, **436**, 33-54 (1992)

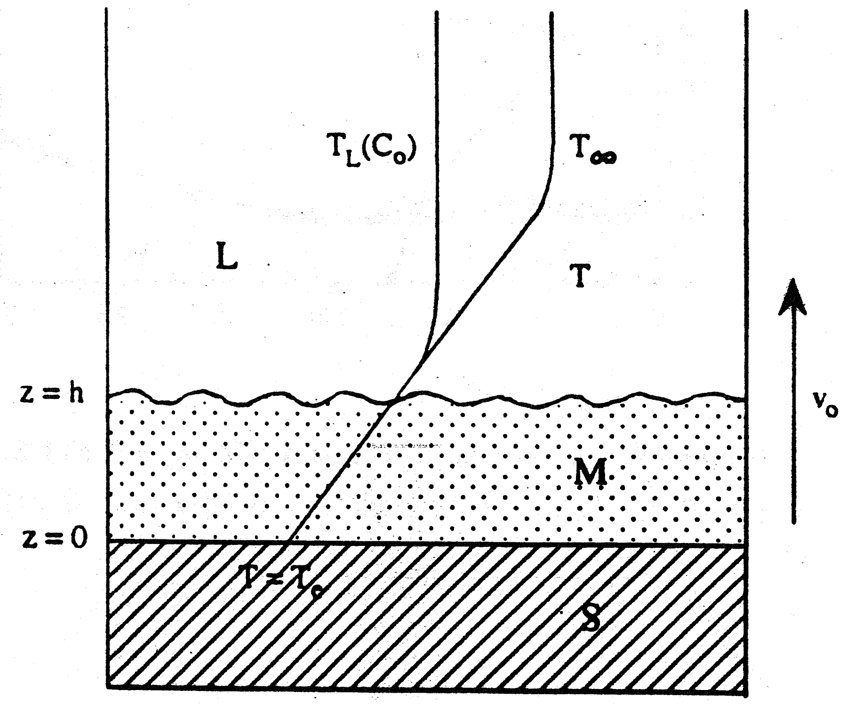

Fig. 1 A diagram representing the directional solidification of an alloy at speed V_0. A mushy layer between a solid region, where temperature $T < T_e$, and a liquid region. The profiles for dimensional temperature and the local liquidus temperature T_L are also shown. L, M and S denote, respectively, liquid, mush and solid regions.

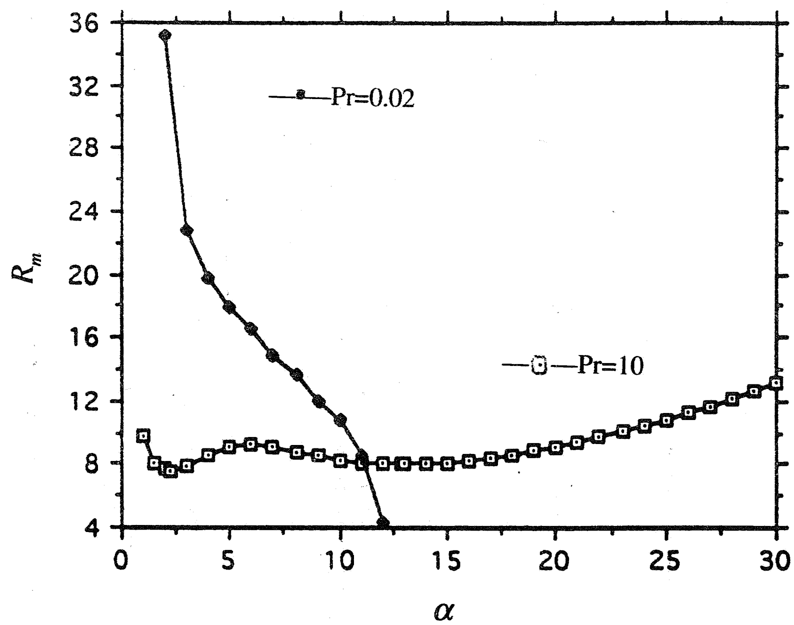

Fig. 2 Marginal stability curves, R_m versus α with $A_m = 0$ and for $Pr = 10$ $(\omega = 0,\ H = 10^5,\ \varepsilon = 0.025)$ and $\mathrm{Pr} = 0.02(\omega = 1.6,\ H = 10^6,\ \varepsilon = 0.01)$.

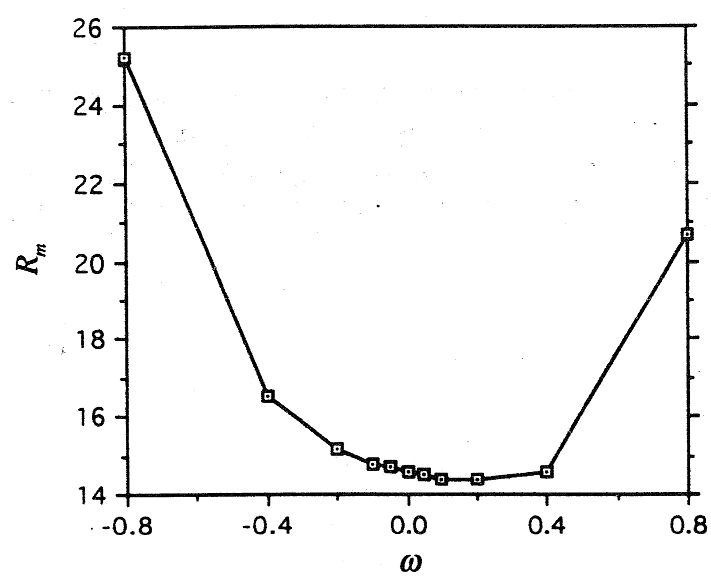

Fig. 3 Marginal stability curve, R_m versus ω, with $A_m = 0.1$ and for $\mathrm{Pr} = 0.02,\ H = 10^6,\ \varepsilon = 0.01,\ \alpha = 2.5$.

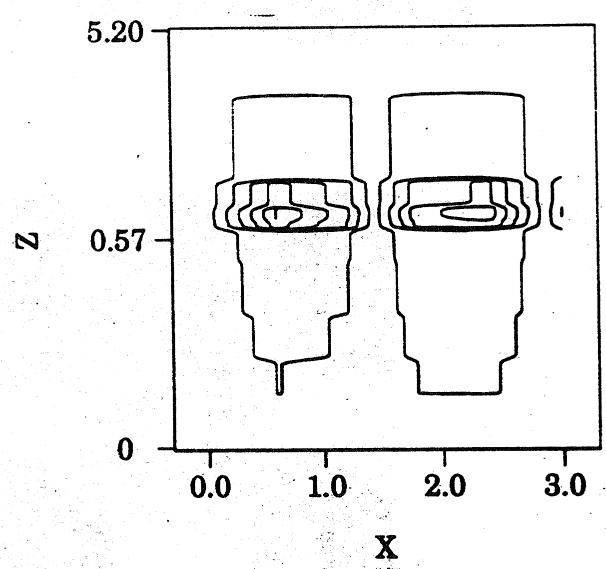

Fig. 4 Streamlines for $A_m = 0$ and for
$Pr = 10$, $H = 10^5$, $\varepsilon = .025$, $\omega = 0$, $\alpha = 2.19$, $R_m = 7.64$.

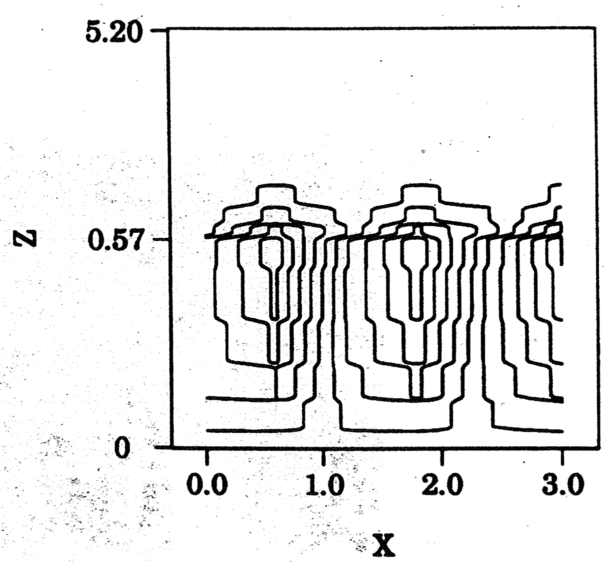

Fig. 5 Streamlines for $A_m = 0.1$ and for
$Pr = 0.02$, $H = 10^6$, $\varepsilon = 0.01$, $\omega = 0.1$, $\alpha = 2.5$, $R_m = 14.4$.

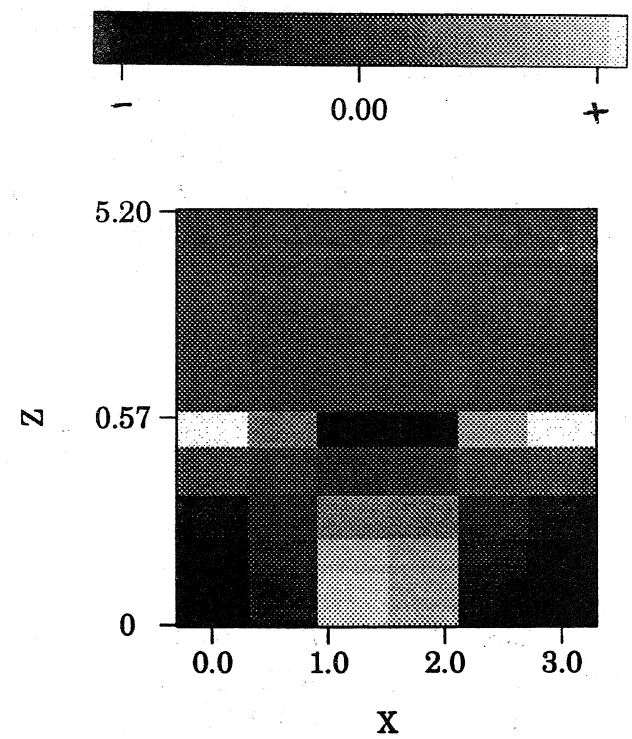

Fig. 6 Density plot of the perturbation to the solid fraction in the mushy region for $A_m = 0$. $\mathrm{Pr} = 10$, $H = 10^5$, $\varepsilon = 0.025$, $\omega = 0$, $\alpha = 2.19$, $\mathrm{R_m} = 7.64$.

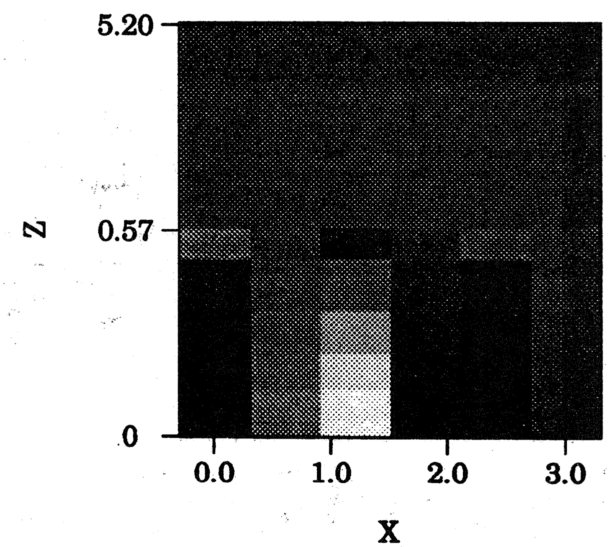

Fig. 7 Density plot of the perturbation to the solid fraction in the mushy region for $A_m = 0.1$. $\mathrm{Pr} = 0.02$, $H = 10^6$, $\varepsilon = 0.01$, $\omega = 0.1$, $\alpha = 2.5$, $\mathrm{R_m} = 14.4$.

List of Recent TAM Reports

No.	Authors	Title	Date
714	Birnbaum, H. K., and P. Sofronis	Hydrogen-enhanced localized plasticity—A mechanism for hydrogen-related fracture	July 1993
715	Balachandar, S., and M. R. Malik	Inviscid instability of streamwise corner flow	July 1993
716	Sofronis, P.	Linearized hydrogen elasticity	July 1993
717	Nitzsche, V. R., and K. J. Hsia	Modeling of dislocation mobility controlled brittle-to-ductile transition	July 1993
718	Hsia, K. J., and A. S. Argon	Experimental study of the mechanisms of brittle-to-ductile transition of cleavage fracture in silicon single crystals	July 1993
719	Cherukuri, H. P., and T. G. Shawki	An energy-based localization theory: Part II—Effects of the diffusion, inertia and dissipation numbers	Aug. 1993
720	Aref, H., and S. W. Jones	Chaotic motion of a solid through ideal fluid	Aug. 1993
721	Stewart, D. S.	Lectures on detonation physics: Introduction to the theory of detonation shock dynamics	Aug. 1993
722	Lawrence, C. J., and R. Mei	Long-time behavior of the drag on a body in impulsive motion	Sept. 1993
723	Mei, R., J. F. Klausner, and C. J. Lawrence	A note on the history force on a spherical bubble at finite Reynolds number	Sept. 1993
724	Qi, Q., R. E. Johnson, and J. G. Harris	A re-examination of the boundary layer attenuation and acoustic streaming accompanying plane wave propagation in a circular tube	Sept. 1993
725	Turner, J. A., and R. L. Weaver	Radiative transfer of ultrasound	Sept. 1993
726	Yogeswaren, E. K., and J. G. Harris	A model of a confocal ultrasonic inspection system for interfaces	Sept. 1993
727	Yao, J., and D. S. Stewart	On the normal detonation shock velocity–curvature relationship for materials with large activation energy	Sept. 1993
728	Qi, Q.	Attenuated leaky Rayleigh waves	Oct. 1993
729	Sofronis, P., and H. K. Birnbaum	Mechanics of hydrogen–dislocation–impurity interactions: Part I—Increasing shear modulus	Oct. 1993
730	Hsia, K. J., Z. Suo, and W. Yang	Cleavage due to dislocation confinement in layered materials	Oct. 1993
731	Acharya, A., and T. G. Shawki	A second-deformation-gradient theory of plasticity	Oct. 1993
732	Michaleris, P., D. A. Tortorelli, and C. A. Vidal	Tangent operators and design sensitivity formulations for transient nonlinear coupled problems with applications to elasto-plasticity	Nov. 1993
733	Michaleris, P., D. A. Tortorelli, and C. A. Vidal	Analysis and optimization of weakly coupled thermo-elasto-plastic systems with applications to weldment design	Nov. 1993
734	Ford, D. K., and D. S. Stewart	Probabilistic modeling of propellant beds exposed to strong stimulus	Nov. 1993
735	Mei, R., R. J. Adrian, and T. J. Hanratty	Particle dispersion in isotropic turbulence under the influence of non-Stokesian drag and gravitational settling	Nov. 1993
736	Dey, N., D. F. Socie, and K. J. Hsia	Static and cyclic fatigue failure at high temperature in ceramics containing grain boundary viscous phase: Part I—Experiments	Nov. 1993
737	Dey, N., D. F. Socie, and K. J. Hsia	Static and cyclic fatigue failure at high temperature in ceramics containing grain boundary viscous phase: Part II—Modeling	Nov. 1993
738	Turner, J. A., and R. L. Weaver	Radiative transfer and multiple scattering of diffuse ultrasound in polycrystalline media	Nov. 1993
739	Qi, Q., and R. E. Johnson	Resin flows through a porous fiber collection in pultrusion processing	Dec. 1993

List of Recent TAM Reports (cont'd)

No.	Authors	Title	Date
740	Weaver, R. L., W. Sachse, and K. Y. Kim	Transient elastic waves in a transversely isotropic plate	Dec. 1993
741	Zhang, Y., and R. L. Weaver	Scattering from a thin random fluid layer	Dec. 1993
742	Weaver, R. L., and W. Sachse	Diffusion of ultrasound in a glass bead slurry	Dec. 1993
743	Sundermeyer, J. N., and R. L. Weaver	On crack identification and characterization in a beam by nonlinear vibration analysis	Dec. 1993
744	Li, L., and N. R. Sottos	Predictions of static displacements in 1–3 piezocomposites	Dec. 1993
745	Jones, S. W.	Chaotic advection and dispersion	Jan. 1994
746	Stewart, D. S., and J. Yao	Critical detonation shock curvature and failure dynamics: Developments in the theory of detonation shock dynamics	Feb. 1994
747	Mei, R., and R. J. Adrian	Effect of Reynolds-number-dependent turbulence structure on the dispersion of fluid and particles	Feb. 1994
748	Liu, Z.-C., R. J. Adrian, and T. J. Hanratty	Reynolds-number similarity of orthogonal decomposition of the outer layer of turbulent wall flow	Feb. 1994
749	Barnhart, D. H., R. J. Adrian, and G. C. Papen	Phase-conjugate holographic system for high-resolution particle image velocimetry	Feb. 1994
750	Qi, Q., W. D. O'Brien Jr., and J. G. Harris	The propagation of ultrasonic waves through a bubbly liquid into tissue: A linear analysis	March 1994
751	Mittal, R., and S. Balachandar	Direct numerical simulation of flow past elliptic cylinders	May 1994
752	Anderson, D. N., J. R. Dahlen, M. J. Danyluk, A. M. Dreyer, K. M. Durkin, J. J. Kriegsmann, J. T. McGonigle, and V. Tyagi	Thirty-first student symposium on engineering mechanics, J. W. Phillips, coord.	May 1994
753	Thoroddsen, S. T.	The failure of the Kolmogorov refined similarity hypothesis in fluid turbulence	May 1994
754	Turner, J. A., and R. L. Weaver	Time dependence of multiply scattered diffuse ultrasound in polycrystalline media	June 1994
755	Riahi, D. N.	Finite-amplitude thermal convection with spatially modulated boundary temperatures	June 1994
756	Riahi, D. N.	Renormalization group analysis for stratified turbulence	June 1994
757	Riahi, D. N.	Wave-packet convection in a porous layer with boundary imperfections	June 1994
758	Jog, C. S., and R. B. Haber	Stability of finite element models for distributed-parameter optimization and topology design	July 1994
759	Qi, Q., and G. J. Brereton	Mechanisms of removal of micron-sized particles by high-frequency ultrasonic waves	July 1994
760	Shawki, T. G.	On shear flow localization with traction-controlled boundaries	July 1994
761	Balachandar, S., D. A. Yuen, and D. M. Reuteler	High Rayleigh number convection at infinite Prandtl number with temperature-dependent viscosity	July 1994
762	Phillips, J. W.	Arthur Newell Talbot—Proceedings of a conference to honor TAM's first department head and his family	Aug. 1994
763	Man., C. S., and D. E. Carlson	On the traction problem of dead loading in linear elasticity with initial stress	Aug. 1994
764	Zhang, Y., and R. L. Weaver	Leaky Rayleigh wave scattering from elastic media with random microstructures	Aug. 1994
765	Cortese, T. A., and S. Balachandar	High-performance spectral simulation of turbulent flows in massively parallel machines with distributed memory	Aug. 1994

List of Recent TAM Reports (cont'd)

No.	*Authors*	*Title*	*Date*
766	Balachandar, S.	Signature of the transition zone in the tomographic results extracted through the eigenfunctions of the two-point correlation	Sept. 1994
767	Piomelli, U.	Large-eddy simulation of turbulent flows	Sept. 1994
768	Harris, J. G., D. A. Rebinsky, and G. R. Wickham	An integrated model of scattering from an imperfect interface	Sept. 1994
769	Hsia, K. J., and Z. Xu	The mathematical framework and an approximate solution of surface crack propagation under hydraulic pressure loading	Sept. 1994
770	Balachandar, S.	Two-point correlation and its eigen-decomposition for optimal characterization of mantle convection	Oct. 1994
771	Lufrano, J. M., and P. Sofronis	Numerical analysis of the interaction of solute hydrogen atoms with the stress field of a crack	Oct. 1994
772	Aref, H., and S. W. Jones	Motion of a solid body through ideal fluid	Oct. 1994
773	Stewart, D. S., T. Aslam, J. Yao, and J. B. Bdzil	Level-set techniques applied to unsteady detonation propagation	Oct. 1994
774	Mittal, R., and S. Balachandar	Effect of three-dimensionality on the lift and drag of circular and elliptic cylinders	Oct. 1994
775	Stewart, D. S., T. D. Aslam, and J. Yao	The evolution of detonation cells	Nov. 1994
776	Aref, H.	On the equilibrium and stability of a row of point vortices	Nov. 1994
777	Cherukuri, H. P., T. G. Shawki, and M. El-Raheb	An accurate finite-difference scheme for elastic wave propagation in a circular disk	Nov. 1994
778	Li, L., and N. R. Sottos	Improving hydrostatic performance of 1–3 piezocomposites	Dec. 1994
779	Phillips, J. W., D. L. de Camara, M. D. Lockwood, and W. C. C. Grebner	Strength of silicone breast implants	Jan. 1995
780	Xin, Y.-B., K. J. Hsia, and D. A. Lange	Quantitative characterization of the fracture surface of silicon single crystals by confocal microscopy	Jan. 1995
781	Yao, J., and D. S. Stewart	On the dynamics of multi-dimensional detonation	Jan. 1995
782	Riahi, D. N., and T. L. Sayre	Effect of rotation on the structure of a convecting mushy layer	Feb. 1995
783	Batchelor, G. K., and TAM faculty and students	A conversation with Professor George K. Batchelor	Feb. 1995
784	Sayre, T. L., and D. N. Riahi	Effect of rotation on flow instabilities during solidification of a binary alloy	Feb. 1995
785	Xin, Y.-B., and K. J. Hsia	A technique to generate straight surface cracks for studying the dislocation nucleation condition in brittle materials	March 1995
786	Riahi, D. N.	Finite bandwidth, long wavelength convection with boundary imperfections: Near-resonant wavelength excitation	March 1995
787	Turner, J. A., and R. L. Weaver	Average response of an infinite plate on a random foundation	March 1995
788	Weaver, R. L., and D. Sornette	The range of spectral correlations in pseudointegrable systems: GOE statistics in a rectangular membrane with a point scatterer	April 1995

List of Recent TAM Reports (cont'd)

No.	*Authors*	*Title*	*Date*
789	Anderson, K. F., M. B. Bishop, B. C. Case, S. R. McFarlin, J. M. Nowakowski, D. W. Peterson, C. V. Robertson, and C. E. Tsoukatos	Thirty-second student symposium on engineering mechanics, J. W. Phillips, coord.	April 1995
790	Figa, J., and C. J. Lawrence	Linear stability analysis of a gravity-driven Newtonian coating flow on a planar incline	May 1995
791	Figa, J., and C. J. Lawrence	Linear stability analysis of a gravity-driven viscosity-stratified Newtonian coating flow on a planar incline	May 1995
792	Cherukuri, H. P., and T. G. Shawki	On shear band nucleation and the finite propagation speed of thermal disturbances	May 1995
793	Harris, J. G.	Modeling scanned acoustic imaging of defects at solid interfaces	May 1995
794	Sottos, N. R., J. M. Ockers, and M. J. Swindeman	Thermoelastic properties of plain weave composites for multilayer circuit board applications	May 1995
795	Aref, H., and M. A. Stremler	On the motion of three point vortices in a periodic strip	June 1995
796	Barenblatt, G. I., and N. Goldenfeld	Does fully-developed turbulence exist? Reynolds number independence versus asymptotic covariance	June 1995
797	Aslam, T. D., J. B. Bdzil, and D. S. Stewart	Level set methods applied to modeling detonation shock dynamics	June 1995
798	Prasad N.B.R. and P. Sofronis	The effect of interface slip and diffusion on the creep strength of fiber and particulate composite materials	July 1995
799	Hsia, K. J., T.-L. Zhang, and D. F. Socie	Effect of crack surface morphology on the fracture behavior under mixed mode loading	July 1995
800	Adrian, R. J.	Stochastic estimation of the structure of turbulent fields	Aug. 1995
801	Riahi, D. N.	Perturbation analysis and modeling for stratified turbulence	Aug. 1995
802	Thoroddsen, S. T.	Conditional sampling of dissipation in high Reynolds number turbulence	Aug. 1995
803	Riahi, D. N.	On the structure of an unsteady convecting mushy layer	Aug. 1995
804	Meleshko, V. V.	Equilibrium of an elastic rectangle: The Mathieu–Inglis–Pickett solution revisited	Aug. 1995
805	Jonnalagadda, K., G. E. Kline, and N. R. Sottos	Local displacements and load transfer in shape memory alloy composites	Aug. 1995
806	Nimmagadda, P. B. R., and P. Sofronis	On the calculation of the matrix–reinforcement interface diffusion coefficient in composite materials at high temperatures	Aug. 1995
807	Carlson, D. E., and D. A. Tortorelli	On hyperelasticity with internal constraints	Aug. 1995
808	Sayre, T. L., and D. N. Riahi	Oscillatory instabilities of the liquid and mushy layers during solidification of alloys under rotational constraint	Sept. 1995